Control of force through feedback in small driven systems

E. Dieterich,[1] J. Camunas-Soler,[2,3] M. Ribezzi-Crivellari,[2,3] U. Seifert,[1] and F. Ritort[2,3]
[1]*II. Institut für Theoretische Physik, Universität Stuttgart, Pfaffenwaldring 57, 70569 Stuttgart, Germany*
[2]*Departament de Física Fonamental, Universitat de Barcelona, Diagonal 647, 08028 Barcelona, Spain*
[3]*CIBER-BBN de Bioingeniería, Biomateriales y Nanomedicina, Instituto de Salud Carlos III, 28029 Madrid, Spain*
(Received 29 February 2016; published 7 July 2016)

Controlling a time-dependent force applied to single molecules or colloidal particles is crucial for many types of experiments. Since in optical tweezers the primary controlled variable is the position of the trap, imposing a target force requires an active feedback process. We analyze this feedback process for the paradigmatic case of a nonequilibrium steady state generated by a dichotomous force protocol, first theoretically for a colloidal particle in a harmonic trap and then with both simulations and experiments for a long DNA hairpin. For the first setup, we find there is an optimal feedback gain separating monotonic from oscillatory response, whereas a too strong feedback leads to an instability. For the DNA molecule, reaching the target force requires substantial feedback gain since weak feedback cannot overcome the tendency to relax towards the equilibrium force.

DOI: 10.1103/PhysRevE.94.012107

I. INTRODUCTION

The advance of experimental techniques allows the study and manipulation of small systems with an unprecedented level of control [1–6]. In particular, force-spectroscopy techniques such as optical and magnetic tweezers are ideally suited to capture and manipulate micrometer-sized objects and measure energies with high accuracy on the order of thermal fluctuations or a few $k_{\mathrm{B}}T$ (with k_B the Boltzmann constant and T the temperature). In these experiments, a mechanical force can be applied to the ends of a molecule tethered between a bead and a surface either by controlling the force or the position. This kind of manipulation opens exciting perspectives in the field of nonequilibrium physics through time-resolved fluctuation spectroscopy measurements. By mechanically perturbing the tethered molecule it is possible to measure time-dependent correlation and response functions using single molecules as model systems. In optical tweezers for instance, the position of the optical trap is controlled by displacing the focus of a laser beam using mechanical or acousto-optic actuators. Optical tweezers are therefore natural position clamps [7]. On the other hand, magnetic tweezers typically work as natural force clamps where the force applied to the beads is controlled by approaching a pair of magnets [8]. However, many biophysical and biochemical experiments require performing both distance-controlled and force-controlled experiments (e.g., follow molecular motors working against a constant load). Feedback mechanisms to perform the latter experiments with optical tweezers have been developed [9,10]. In fact, although passive force clamps can also be achieved with optical tweezers [11], most optical tweezers setups achieve force control using active feedback mechanisms in which the position of the optical trap is adjusted at rates $\sim$10 Hz–1 kHz to keep the force constant [7,10,12]. Such active feedback mechanisms have been particularly useful to characterize a variety of biophysical systems such as folding of nucleic acids structures, processive DNA motors, or force-dependent kinetics of ligand binding [13–16]. Consequently, an accurate characterization and understanding of the parameters driving active feedback systems is essential for an appropriate interpretation of many single-molecule experimental results. In turn, the development of feedback systems has provided the means to investigate fundamental aspects of the nonequilibrium physics of small systems such as experimental realizations of the Maxwell demon [17,18] and the verification of Landauer's principle [19–21], or the observation of effective temperatures in driven DNA molecules [22]. In addition, experimental progress in these systems has prompted the development of theoretical descriptions of feedback mechanisms for small systems and further refinement in the theory of feedback control [23–29].

Here, we study a force feedback protocol for optical tweezers setups, which randomly changes the force in a dichotomous fashion between a lower and a higher force value. This stochastic protocol drives the system to a nonequilibrium steady state that, under well-defined conditions, has been shown to fulfill the fluctuation-dissipation theorem but with an effective temperature higher than the bath temperature, mimicking additional thermal noise arising from the random forcing [22]. In the following, we first introduce the experimental setup and the force feedback (Sec. II). We then discuss a toy model in which the force feedback mechanism is implemented for a harmonic oscillator (Sec. III). Subsequently, we investigate force feedback for a stochastically driven DNA hairpin in both theory and experiments (Sec. IV). Finally, we conclude by summarizing our main results and emphasizing how the mechanical un(folding) of single molecules provides a paradigmatic example to discuss theoretical concepts in the field of feedback-controlled small systems.

II. EXPERIMENTAL SETUP AND FEEDBACK

A. Free-energy landscape

In the experimental setup, a bead is attached to each strand of a DNA hairpin of 6800 base pairs via molecular handles, in our case short segments (29 base pairs) of double-stranded DNA. One of the beads is captured with an optical trap while the other one is kept immobilized by air suction in the tip of a glass pipette [see Fig. 1(a)]. By controlling the position λ of the optical trap, a force f is applied on the DNA hairpin. The application of a larger force unfolds the DNA, thereby increasing the number of open base pairs n. Figure 1(b) shows

 ©2016 American Physical Society

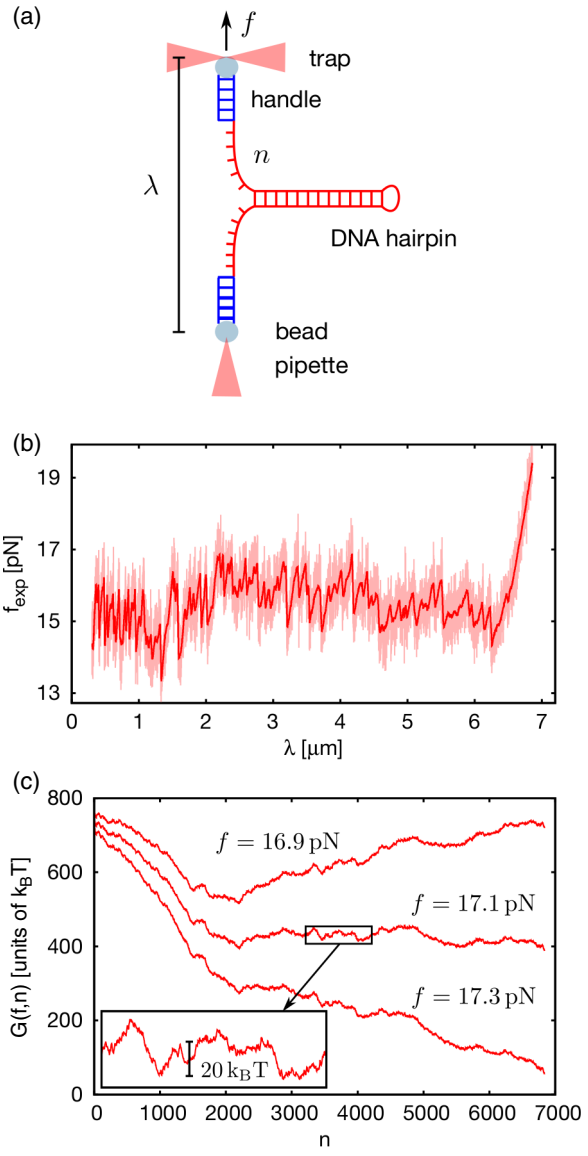

FIG. 1. (a) Experimental DNA unfolding setup. Moving the optical trap with position λ changes the force f, which is applied on the DNA hairpin. A larger force unfolds the DNA, i.e., increases the number of open base pairs n. (b) Experimental force-distance curve of the 6800 base pairs DNA hairpin for a protocol that increases the trap position λ linearly in time with speed $v = 300\,\mathrm{nm/s}$ (unfiltered data at 1 kHz in lighter color and data filtered at 4 Hz in darker color). The relation between the measured force f_{exp} and the actual force f is given by Eq. (1). (c) Free-energy profile $G(f,n)$ of the hairpin versus the number of open base pairs n for various values of the force f.

the force-distance curve (FDC) obtained by increasing the trap position linearly in time while measuring the force applied to the ends of the hairpin. This FDC shows a typical sawtoothlike pattern representing the unfolding reaction of the DNA hairpin as it progresses through many partially unfolded intermediate states.

Intermediate states are expected from the predicted free-energy profile of the hairpin, which can be derived from its FDC [30]. In Fig. 1(c), we show the free-energy profile for several values of the force f around the coexistence force ($f_c \simeq 17.1\,\mathrm{pN}$), the latter being defined as that value of the force where the state with $n \simeq 2000$ and the fully unfolded state have equal free energies. The 6800 base pairs DNA hairpin has many intermediate states that are separated by barriers much larger than $k_{\mathrm{B}}T$. Moreover, at the coexistence force, the free energy drops sharply for roughly the first 2000 base pairs of the hairpin due to the high abundance of AT base pairs in that region. Consequently, in our experiments and simulations, the long hairpin is rarely seen to fold below $n \simeq 2000$ at forces not far from f_c. Finally, we stress that the application of a force $f > f_c$ tilts the free-energy profile such that unfolded states become energetically more favored. Changing the force over time, as in the stochastic driving we are considering here, thus drives the hairpin back and forth across its free-energy profile.

B. Constant force feedback

So far, we have discussed the free-energy profile of the hairpin for various controlled values of the force f. However, in experiments with optical tweezers, one controls the position λ of the trap whereas the force f fluctuates. To nevertheless control the force, a feedback protocol is implemented by the repeated execution of the following two steps:

Step 1. The force f that acts against the captured bead is measured as an average over a time interval τ_F

$$f_{\mathrm{exp}} \equiv \frac{1}{\tau_F}\int_0^{\tau_F} f(t)\,dt, \tag{1}$$

where f_{exp} is the experimentally recorded force and the initial time 0 is taken at the beginning of the time interval.

Step 2. The optical trap is moved depending on the measurement outcome to bring this force closer to a target value f_T. More precisely, given some measured force f_{exp} as input, the feedback adjusts the trap position λ by means of

$$\Delta\lambda = G\frac{f_T - f_{\mathrm{exp}}}{k_{\mathrm{eff}}}, \tag{2}$$

where G is the dimensionless feedback gain and where k_{eff} is an effective rigidity of fixed value, which sets the relevant scale for the conversion from forces to distances. Hence, if the force is smaller than the desired value f_T, the feedback increases the distance λ to pull stronger ($\Delta\lambda > 0$). Conversely, if f_{exp} is larger than f_T, $\Delta\lambda < 0$ to decrease the force. How much the trap is moved in these two cases is determined by the feedback gain G, which is a free parameter of the force feedback.

Ideally, this feedback might be used to apply and maintain a constant force on the DNA. In Fig. 2, we show data for experiments which start with the DNA hairpin in the folded state and use the feedback defined by Eq. (2) to apply a constant force sufficiently large to completely unfold the DNA. Figure 2(a) illustrates that whenever the force f_{exp} drops below the target value f_T, the feedback increases the trap position λ, in agreement with Eq. (2). Furthermore, Fig. 2(b) demonstrates that the hairpin remains stuck in several intermediate states for a noticeable time before unfolding into the next intermediate. This result is in agreement with the earlier observation that the intermediate states are separated by large barriers if a constant force is applied [see Fig. 1(c)]. Moreover, the varying

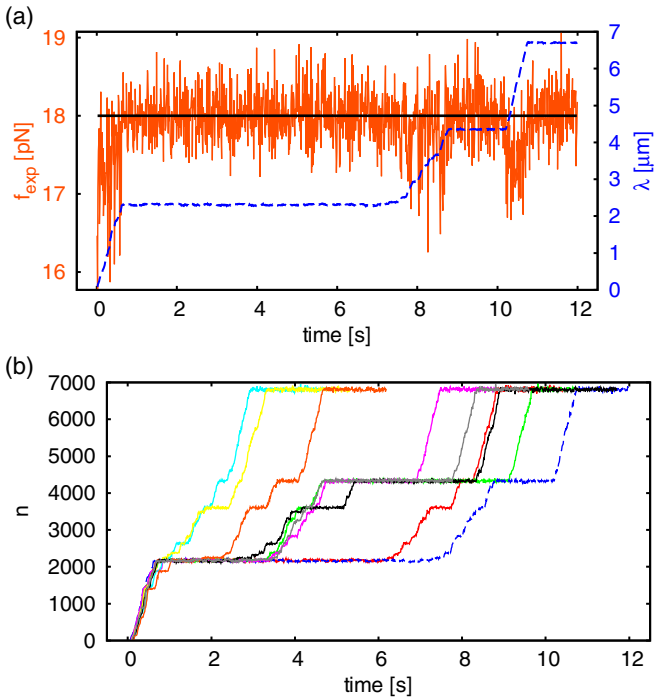

FIG. 2. (a) Experimental trajectory of the force $f_{\rm exp}$ (solid, lighter color) and the trap position λ (dashed) using the linear feedback defined in Eq. (2) to apply a constant force (black). (b) Trajectories of the number of open base pairs n for different repetitions of the experiment each using the same feedback protocol as in (a). The dashed curves in (a) and (b) correspond to the same experiment.

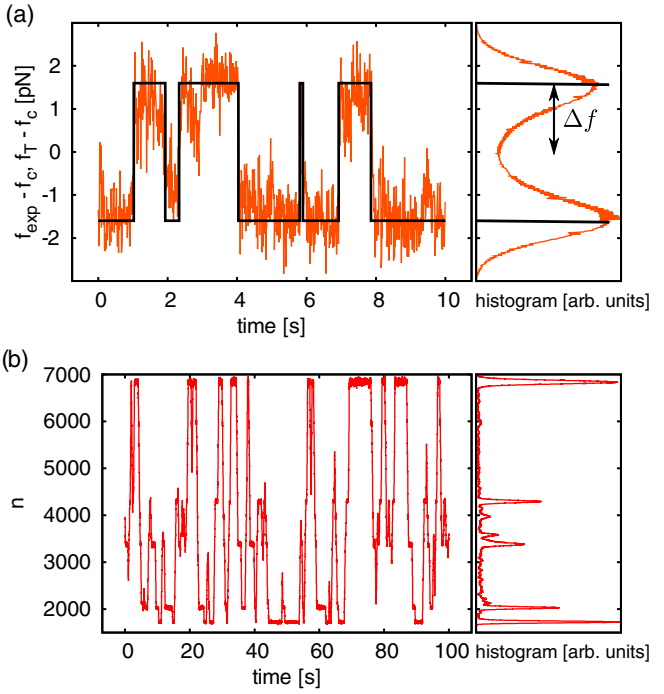

FIG. 3. (a) Experimental trajectory segment (left) and histogram (right) of the target force f_T (black) and the force $f_{\rm exp}$ (lighter color), where $k_{\rm eff} \simeq 0.1\,$pN/nm, $f_c = 18.1\,$pN, $\Delta f = 1.6\,$pN, $\tau_e = 1.33\,$s, $\tau_F = 1\,$ms, and $G = 1$. (b) Corresponding trajectory segment (left) and histogram (right) of the number of open base pairs n. In both (a) and (b), the histogram is evaluated over the full trace from which the time segment shown on the left hand side has been excerpted. This trace is 1280 s long.

amounts of time spent in a given intermediate across different constant force experiments highlight the stochastic nature of the unfolding process.

C. Stochastic driving

The discussion of the constant force feedback has shown that the DNA hairpin remains stuck in one state if a constant force is applied, since large barriers in the free-energy profile prevent further transitions [see Fig. 1(c) and Fig. 2(b)]. In the following, we discuss a protocol that changes the target force over time and thus helps the DNA to continuously perform transitions among many of its states. Specifically, we consider the case of a dichotomous stochastic target force that is randomly switched at a rate $1/\tau_e$ between the two values

$$f_T^{\pm} \equiv f_c \pm \Delta f, \tag{3}$$

where f_c is the mean force and Δf the force amplitude. For this protocol, Fig. 3(a) illustrates how the feedback adjusts the force $f_{\rm exp}$ to the stochastic target force f_T. Since the feedback control is not perfect, the force fluctuates noticeably around the target value. However, for the feedback parameters considered in Fig. 3, these fluctuations are small compared to the force amplitude Δf of the external protocol. We furthermore stress that this protocol indeed drives the DNA hairpin back and forth through its states [see Fig. 3(b)].

In the following, the feedback-controlled dynamics of the stochastically driven hairpin will be systematically explored in both theory and experiment. In Sec. III we consider a toy model of force feedback and study the feedback-controlled dynamics of an overdamped particle in a harmonic oscillator. For this system, we investigate the average reaction of the force to a change of the target value during the stochastic driving. In Sec. IV A, this quantity is discussed in the context of the DNA hairpin system under random forcing. Subsequently, the dynamics of the DNA hairpin under force feedback is further evaluated through contour plots of the probability density in the $(f_{\rm exp},\lambda)$ plane (Sec. IV B).

III. TOY MODEL: HARMONIC OSCILLATOR

A. Feedback

We consider the dynamics of an overdamped particle in the harmonic trap $V(x,\lambda) = k(x-\lambda)^2/2$ where x and λ are the positions of the particle and the trap, respectively, and where k is the trap stiffness. The dynamics of this system can be described by the Langevin equation

$$\dot{x} = -\mu\partial_x V(x,\lambda) + \zeta(t), \tag{4}$$

where μ is the mobility and $\zeta(t)$ the thermal white noise with mean $\langle\zeta(t)\rangle_{\rm th} = 0$ and variance $\langle\zeta(t_2)\zeta(t_1)\rangle_{\rm th} = 2\mu k_B T\delta(t_2 - t_1)$. For this system, the force feedback is implemented in analogy to the DNA unfolding system. Hence, we model a feedback that repeatedly first measures the force $f = -k(x-\lambda)$ that acts on the particle and then adjusts the position λ of the trap according to Eq. (2) in order to bring f closer to the desired

target force f_T. The feedback needs a finite operation time τ_F during which the trap position is kept constant to perform each one of these measurements. All force measurements thus represent a time average over one time interval τ_F.

Let the initial trap position at time $t = 0$ be λ_0. The dynamics of the trapped particle is then governed by

$$\dot{x} = -(x - \lambda_0)/\tau_s + \zeta(t) \tag{5}$$

in the following time interval $0 \leqslant t < \tau_F$, where $\tau_s \equiv 1/(\mu k)$ is the relaxation time of the particle in the trap. In this time interval, within the feedback scheme, the mean force [see Eq. (1)]

$$f_0 \equiv \frac{1}{\tau_F} \int_0^{\tau_F} f(t)\, dt \tag{6}$$

is measured first and then, at time $t = \tau_F$, the trap position is instantaneously changed to the new value

$$\lambda_1 = G \frac{f_T - f_0}{k} + \lambda_0 \tag{7}$$

[see Eq. (2)]. This procedure is repeated in the following feedback interval but with the trap position updated to λ_1. For any given external protocol of the target force $f_T(t)$, the feedback-controlled dynamics can therefore be solved in an iterative manner. Here, we use the same protocol as for the DNA unfolding system but with $f_c = 0$, hence, we randomly switch the target force between the two values $\pm\Delta f$ at rate $1/\tau_e$ [see Eq. (3)].

B. Feedback-induced relaxation towards the target force

Whenever the external protocol changes the target force during the stochastic driving, the feedback needs to adjust the force to a new value. The feedback thus induces a reaction of the force to a change of the target value, which depends critically on the feedback parameters and can therefore be used to characterize the feedback. Since the target force is random and because of the presence of thermal noise, the force reacts stochastically to a jump of the target force [see Fig. 4(a)]. In the following, we hence consider the average reaction of the force to a given change of the target value along the particle trajectory. Specifically, from now on, we focus on transitions of the target force from $f_T^- = -\Delta f$ to $f_T^+ = \Delta f$ [$f_c = 0$ in Eq. (3)] noting that for the opposite transition, $f_T^+ = \Delta f$ to $f_T^- = -\Delta f$, the results are the same except for an overall change of sign.

The average that we perform is illustrated in Fig. 4(a). For this average, we introduce a time τ to describe the position of the oscillator along a given time interval where the target force has been set to $f_T^+ = \Delta f$. We will call this an f_T^+ time interval or f_T^+ interval for short. Now let t_0 be the time at the beginning of such an f_T^+ interval, i.e., the time at which the target force changes from $-\Delta f$ to Δf. For a given f_T^+ interval, we start counting τ from zero at time $t = t_0 - \tau_F$ [Fig. 4(a)]. For that f_T^+ interval, the time τ is taken to run from zero till the time at which the protocol changes the target force back to $-\Delta f$. For a given value of τ, the average is then performed over all f_T^+ intervals. In analogy to τ we also introduce, for a given f_T^+ interval, the discrete variable j to keep track of the number of feedback subintervals (each of duration τ_F) elapsed since the target value was changed from f_T^- to f_T^+. For example, the first subinterval $j = 0$ denotes the trajectory of the oscillator for $0 < \tau < \tau_F$ in a given f_T^+ interval. We will use this discrete variable to determine the mean force in

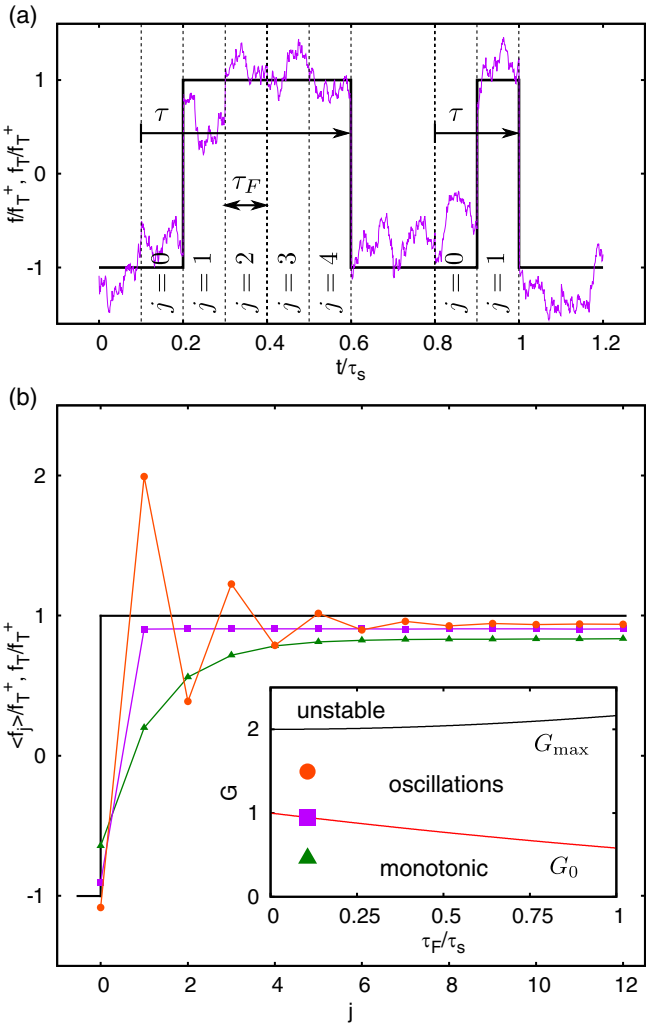

FIG. 4. (a) Simulated trajectory of the force $f = -k(x - \lambda)$ on the particle (lighter color) and the target force of the feedback (black) for $f_T^+/\sqrt{kk_BT} = 1$, $\tau_F/\tau_s = 0.1$, $\tau_e/\tau_s = 0.4$, and $G \simeq 0.95$. Whenever the target force is changed from the bottom to the top value, we start measuring the time τ and the number j of feedback iterations from zero one time interval τ_F in advance. Note that the feedback updates the target force f_T after each iteration and thus does not react immediately to changes of f_T. Performing an average of the force f over all feedback iterations with the same value of j leads to the curve with squares shown in (b). (b) Mean force $\langle f_j \rangle$ in the jth feedback interval [Eq. (19)] after a change of the target force (black) for the same τ_F/τ_s and τ_e/τ_s as in (a) and with $G = 1.5$ (circles), $G = G_0 \simeq 0.95$ (squares), and $G = 0.5$ (triangles). For each G, the value of $\langle f_0 \rangle$ has been determined numerically from simulations of the feedback-controlled dynamics. As a guide for the eyes, we have drawn lines connecting the values of $\langle f_j \rangle$. The inset shows the maximal feedback gain $G_{\max}$ [Eq. (18)] and the optimal feedback gain G_0 [Eq. (21)]. With symbols in corresponding shape, we mark the combinations of G and τ_F/τ_s for which the mean force $\langle f_j \rangle$ is plotted in the main panel.

the jth feedback subinterval after a change of the target force from f_T^- to f_T^+.

We stress that the target force that the protocol dictates and the thermal noise that the particle feels are not correlated. Therefore, the above introduced average can be analytically performed by separately first carrying out the thermal average for one f_T^+ interval and then running the average over all f_T^+ intervals, which occur along the external protocol. We assume that for the single f_T^+ interval, which we consider first, the positions of the particle and trap at time $\tau = 0$ are $x(0)$ and λ_0, respectively, so that the force at that time is $f(0) = -k[x(0) - \lambda_0]$. Then, referring to the thermal average again by $\langle \dots \rangle_{\rm th}$, we find

$$\langle x(\tau)\rangle_{\rm th} = [x(0) - \lambda_0]\exp(-\tau/\tau_s) + \lambda_0 \tag{8}$$

for all times $0 \leqslant \tau < \tau_F$ by solving Eq. (5). We note that the thermal noise $\zeta(\tau)$ enters the particle trajectory $x(\tau)$ linearly for the harmonic oscillator and is thus canceled by the thermal average. From the above Eq. (8), we obtain

$$\langle f(\tau)\rangle_{\rm th} = -k[\langle x(\tau)\rangle_{\rm th} - \lambda_0] = f(0)\exp(-\tau/\tau_s) \tag{9}$$

as the force trajectory for all times $0 \leqslant \tau < \tau_F$ in one given f_T^+ interval of the target force where the initial force at time $\tau = 0$ is $f(0)$. Since for any other f_T^+ interval, only the initial force $f(0)$ is different, the average over all of these intervals along the protocol simply acts as an average over the initial force $f(0)$. We therefore find

$$\langle f(\tau)\rangle = \langle f(0)\rangle \exp(-\tau/\tau_s), \tag{10}$$

for all times $0 \leqslant \tau < \tau_F$, where $\langle \dots \rangle$ represents the average over all f_T^+ intervals which occur along the protocol. The mean force for all times $0 \leqslant \tau < \tau_F$ follows as

$$\langle f_0\rangle \equiv \frac{1}{\tau_F}\int_0^{\tau_F} \langle f(\tau)\rangle\, d\tau = \frac{\langle f(0)\rangle \tau_s}{\tau_F}[1 - \exp(-\tau_F/\tau_s)]. \tag{11}$$

The feedback uses this force to calculate with

$$\langle \lambda_1\rangle \equiv G\frac{f_T^+ - \langle f_0\rangle}{k} + \langle \lambda_0\rangle \tag{12}$$

the mean new position of the trap during the next feedback sub interval $\tau_F \leqslant \tau < 2\tau_F$ [see Eq. (7), where $f_T = f_T^+$ since we consider f_T^+ intervals]. The mean force at time $\tau = \tau_F$ then is

$$\langle f(\tau_F)\rangle = -k[\langle x(\tau_F)\rangle - \langle \lambda_1\rangle] = \langle f(0)\rangle\alpha + Gf_T^+, \tag{13}$$

where

$$\alpha \equiv \exp(-\tau_F/\tau_s) - \frac{G\tau_s}{\tau_F}[1 - \exp(-\tau_F/\tau_s)]. \tag{14}$$

The average force in the feedback subinterval $\tau_F \leqslant \tau < 2\tau_F$ follows as

$$\begin{aligned}\langle f_1\rangle &= \frac{1}{\tau_F}\int_{\tau_F}^{2\tau_F} \langle f(\tau_F)\rangle \exp[-(\tau - \tau_F)/\tau_s]\, d\tau \\ &= \langle f_0\rangle\alpha + \frac{Gf_T^+\tau_s}{\tau_F}[1 - \exp(-\tau_F/\tau_s)].\end{aligned} \tag{15}$$

This calculation can be iterated to get the mean force in the jth feedback subinterval

$$\langle f_j\rangle = \langle f_0\rangle\alpha^j + \frac{Gf_T^+\tau_s}{\tau_F}[1 - \exp(-\tau_F/\tau_s)]\sum_{m=0}^{j-1}\alpha^m, \tag{16}$$

shown in Fig. 4(b). In the limit $j \to \infty$, this force converges to a finite value only if

$$|\alpha| < 1. \tag{17}$$

For a given feedback time τ_F, this condition is matched for feedback gains $G < G_{\rm max}$ with

$$G_{\rm max} \equiv \frac{\tau_F}{\tau_s}\frac{1 + \exp(-\tau_F/\tau_s)}{1 - \exp(-\tau_F/\tau_s)}. \tag{18}$$

The mean force in the jth feedback sub interval then converges with

$$\langle f_j\rangle = \langle f_\infty\rangle + \alpha^j(\langle f_0\rangle - \langle f_\infty\rangle) \tag{19}$$

to the limit force

$$\langle f_\infty\rangle \equiv \lim_{j\to\infty}\langle f_j\rangle = \frac{Gf_T^+}{\tau_F/\tau_s + G}. \tag{20}$$

For the optimal feedback gain

$$G_0 \equiv \frac{\tau_F}{\tau_s}\frac{\exp(-\tau_F/\tau_s)}{1 - \exp(-\tau_F/\tau_s)} \tag{21}$$

α becomes zero so that the mean force $\langle f_j\rangle$ is equal to the limit value $\langle f_\infty\rangle$ right after the first feedback adjustment [see Eq. (19) and Fig. 4(b)]. For smaller feedback gains $G < G_0$, α is positive (but smaller than one) and therefore, $\langle f_j\rangle$ converges monotonically towards $\langle f_\infty\rangle$. For larger feedback gains $G_0 < G < G_{\rm max}$, α is negative (but larger than minus one) so that $\langle f_j\rangle$ shows damped oscillations around the limit value $\langle f_\infty\rangle$ [see Fig. 4(b)]. In this case, the feedback adjustments are strong enough to let $\langle f_j\rangle$ surpass its target value. These oscillations get stronger the more the feedback gain approaches the threshold value $G_{\rm max}$. Ultimately, for $G > G_{\rm max}$, i.e., $\alpha < -1$, the feedback adjustments are so strong that the mean force $\langle f_j\rangle$ is farther away from the target value after each feedback iteration. The oscillations of $\langle f_j\rangle$ then grow over time and the system is unstable [see Eq. (19)].

This analysis of the force feedback for the harmonic oscillator shows that the time evolution of the mean force after a change of the target force depends crucially on which feedback gain G and feedback operation time τ_F is used, as summarized in the phase diagram shown as inset in Fig. 4(b). Specifically, G and τ_F also determine the limit value $\langle f_\infty\rangle$ to which the mean force $\langle f_j\rangle$ converges if $G < G_{\rm max}$ [see Eq. (20)]. This limit value is below f_T^+ for all G and τ_F since the particle inevitably tends to relax towards the minimum of the trap where the force is zero. This result becomes particularly transparent if the limiting mean force, Eq. (20), is evaluated for the optimal feedback gain G_0 for which

$$\langle f_\infty\rangle = f_T^+\exp(-\tau_F/\tau_s). \tag{22}$$

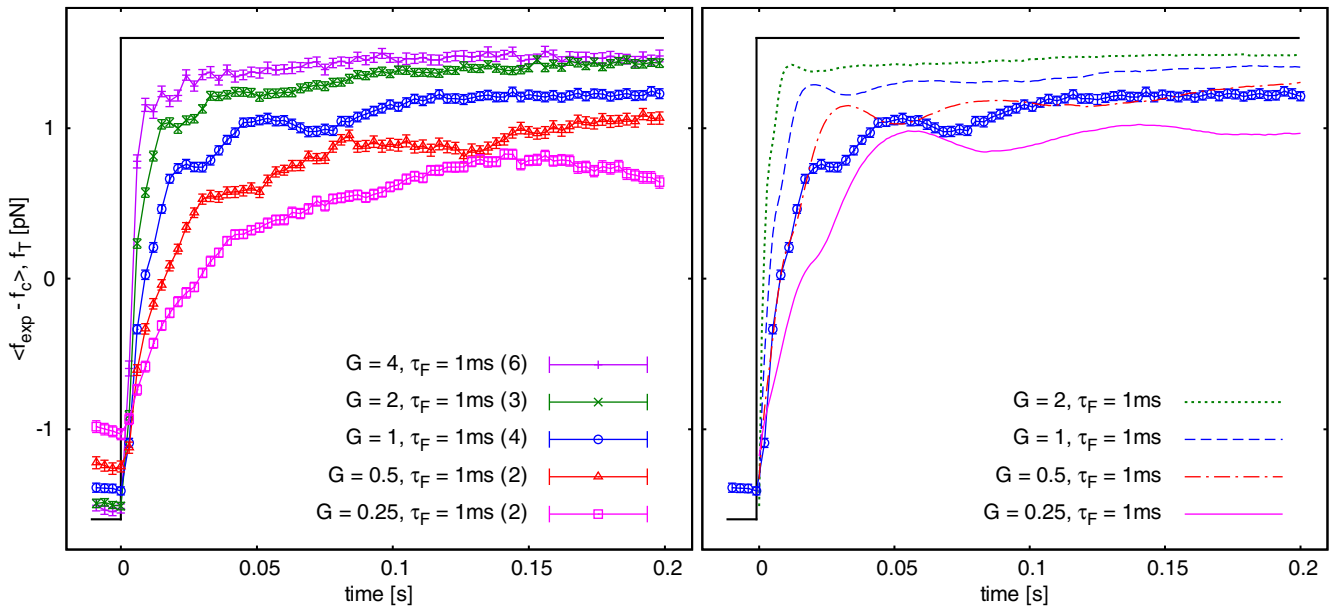

FIG. 5. Experimental (left) and simulated (right) force relaxation after a change of the target force from $f_T^- = f_c - \Delta f$ to $f_T^+ = f_c + \Delta f$ (black), for $\Delta f = 1.6\,\mathrm{pN}$, $\tau_e = 1.33\,\mathrm{s}$, $\tau_F = 1\,\mathrm{ms}$ and various G. The value of f_c is different in theory ($f_c = 17.0\,\mathrm{pN}$) and experiment ($f_c \simeq 18.1\,\mathrm{pN}$) but is similar to the respective mean unzipping force in both cases. All experimental results are single molecule averages over a different number of single molecules. For each value of G, this number is given in brackets in the legend. The experimental result for $G = 1$ is plotted in both the left and the right panel.

IV. DNA UNFOLDING

A. Feedback-induced relaxation towards the target force

We start the discussion of the force feedback in the DNA unfolding setup by considering the force relaxation after a change of the target force as discussed above for the harmonic oscillator. Figure 5 shows the experimental force relaxation for the stochastically driven hairpin using various feedback gains G. The experimental results for different single molecules at the same value of G agree remarkably well, thus proving the consistency of the data (see Fig. 8 in the Appendix). Moreover, the experiments show that increasing G leads to a faster convergence of the mean force to the new target value. This result suggests that the experiments have been performed in the monotonic regime identified for the harmonic oscillator (inset of Fig. 4). However, the experiments clearly show that the convergence of the mean force is not strictly monotonic but instead shows gentle oscillations. These oscillations reflect the fact that the (un)folding process of the DNA hairpin occurs on more than one time scale, in contrast to the particle in the harmonic oscillator that relaxes on a single time scale. In fact, while the feedback just needs to react to the dynamics of a few base pairs for short times, big transitions involving cooperatively unzipping regions containing a large number of base pairs (from several tens to a few hundred, see Ref. [31]) contribute to the feedback response over longer times. Since the feedback needs some time to respond to these large unzipping transitions, the mean force first drops and then rises again. The oscillations of the force relaxation illustrate that this process takes place on several time scales.

We support these experimental results by simulations of the dynamics of the DNA hairpin, which explicitly include the feedback mechanism according to Eq. (2) but otherwise follow an earlier scheme described in detail elsewhere [22]. Briefly, the simulations use Kramers-type rates for the opening and closing of a single base pair within the free-energy profile $G(\lambda(t),n)$ of the hairpin. This free-energy profile can be calculated from a theoretical model of the unfolding setup [30], which we have already used above to display the free energy $G(f,n)$ in Fig. 1(c). The time dependence of the trap position $\lambda(t)$ is determined by the feedback mechanism, which periodically performs adjustments of λ according to Eq. (2) to reach the target force f_T.

Figure 5 shows that there is qualitative agreement of the simulated and experimental force relaxation after a change of the target value. Specifically, the mean force converges faster towards the target value for larger feedback gains G in both theory and experiment. Moreover, the simulated force relaxation shows oscillations, which are similar to those reported in the experiments. However, despite their qualitative agreement, theory and experiment also show visible differences in that the simulated force is systematically closer to the target value f_T for the same value of G (right-hand side of Fig. 5). Therefore, the value of G at which the force f_{exp} overshoots the target force and for which the system becomes unstable is smaller in the simulations. Indeed, the feedback gain $G = 4$, which experimentally leads to a quick convergence of the mean force causes the force to show oscillations, which grow over time in the simulations without ever converging. Hence, the simulation result for $G = 4$ is not shown in Fig. 5.

The deviations between theory and experiment are caused by experimental limitations of the feedback, one of them being that the trap position cannot be adjusted instantaneously to a new value since the trap moves at a finite speed (due to the finite time response of the fiber wiggler that is

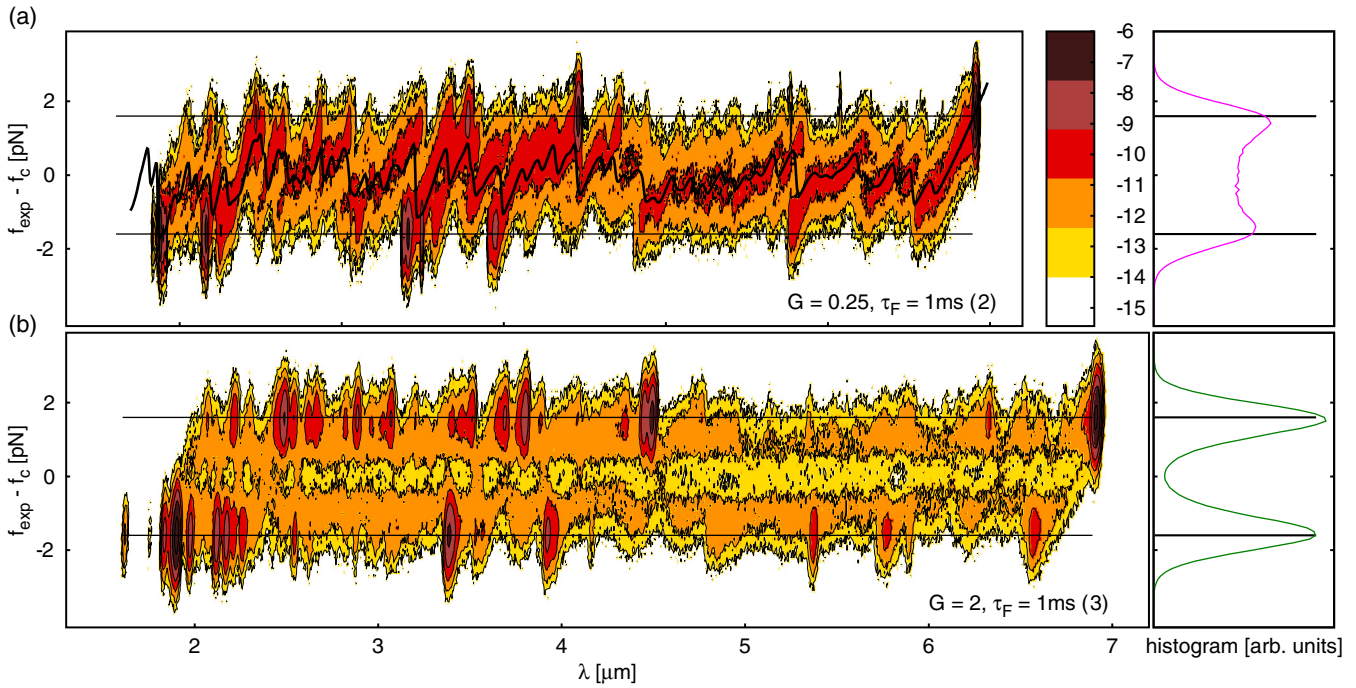

FIG. 6. Logarithm of the experimental probability density in the ($f_{\rm exp}$,λ) plane (left) and corresponding force histogram (right) for $f_c \simeq 18.1$ pN, $\Delta f = 1.6$ pN, $\tau_e = 1.33$ s, $\tau_F = 1$ ms and two values of the feedback gain G. In (a), we show the equilibrium FDC in black. The target values are represented by horizontal lines. All results are averages over single molecules (their number is given in brackets in each panel).

mechanically coupled to the piezo crystal). These effects have not been included in our simulations, indicating that the earlier identified oscillations of the force relaxation are not caused by the specifics of the experimental feedback but are rooted in the multiple time scales of the DNA hairpin.

B. Probability density in the ($f_{\rm exp}$,λ) plane

The above discussion of the feedback-induced relaxation of the force towards its target value has shown that the DNA relaxes on multiple time scales, causing the force to drop repeatedly before being readjusted by the feedback. In the following, this relaxation process of the DNA when subject to feedback control will be discussed in more detail by considering the probability density in the ($f_{\rm exp}$,λ) plane.

Figure 6(a) displays the experimental probability density in the ($f_{\rm exp}$,λ) plane for a small feedback gain G. The gross features of this probability density can be understood when considering the mean measured FDC upon quasireversibly unfolding the DNA hairpin by increasing the trap position λ very slowly without any feedback [black curve in Fig. 6(a), this FDC can be derived from the free-energy profile displayed in Fig. 1(c)]. Since the system can equilibrate for each value of λ in this case, this FDC gives the mean equilibrium force for each trap position λ. For the force feedback considered here, λ is permanently changed to adjust the force $f_{\rm exp}$ to the target value f_T. Yet, within each feedback interval with length τ_F, the trap position λ is kept constant. Hence, in each feedback interval, the system tends to relax to the equilibrium state that corresponds to the current trap position λ. As a consequence, on average the force $f_{\rm exp}$ drifts towards the equilibrium value as given by the FDC. This inevitable relaxation of the feedback-controlled DNA hairpin is analogous to that of the overdamped particle towards the minimum of the trap observed in Sec. III [see Eqs. (20) and (22)].

For the stochastic driving, the target force f_T is either above or below the equilibrium force to ensure that the hairpin is driven back and forth across the majority of its intermediates (see Fig. 6). By trying to adjust the force to the target values, the feedback thus competes with the relaxation of the force towards its equilibrium value, which takes place within each feedback interval. The parameters of the feedback determine the outcome of this competition, i.e., by how much the DNA hairpin is pushed into the nonequilibrium regime. The experiment shown in Fig. 6(a) demonstrates that if the feedback gain G is small, i.e., if the feedback adjustments are weak, the system is hardly driven out of equilibrium so that only forces in the proximity of the FDC are populated. For a larger G on the other hand, Fig. 6(b) shows that the feedback can better counteract the relaxation of the DNA into equilibrium so that the force population is pushed towards the target forces. This observation complements the earlier result that increasing G leads to a faster convergence of the mean force to its target value (Fig. 5).

The change of the force distribution upon increasing the feedback gain G can be further characterized when considering the histograms over the experimental traces of the force $f_{\rm exp}$ [Figs. 6(a) and 6(b)]. These force histograms demonstrate that the variance of the force for a given target force f_T becomes smaller if the feedback gain G gets larger. In particular, for $G = 2$, the force variance is small compared to the amplitude Δf of the random forcing [Eq. (3)], which the feedback attempts

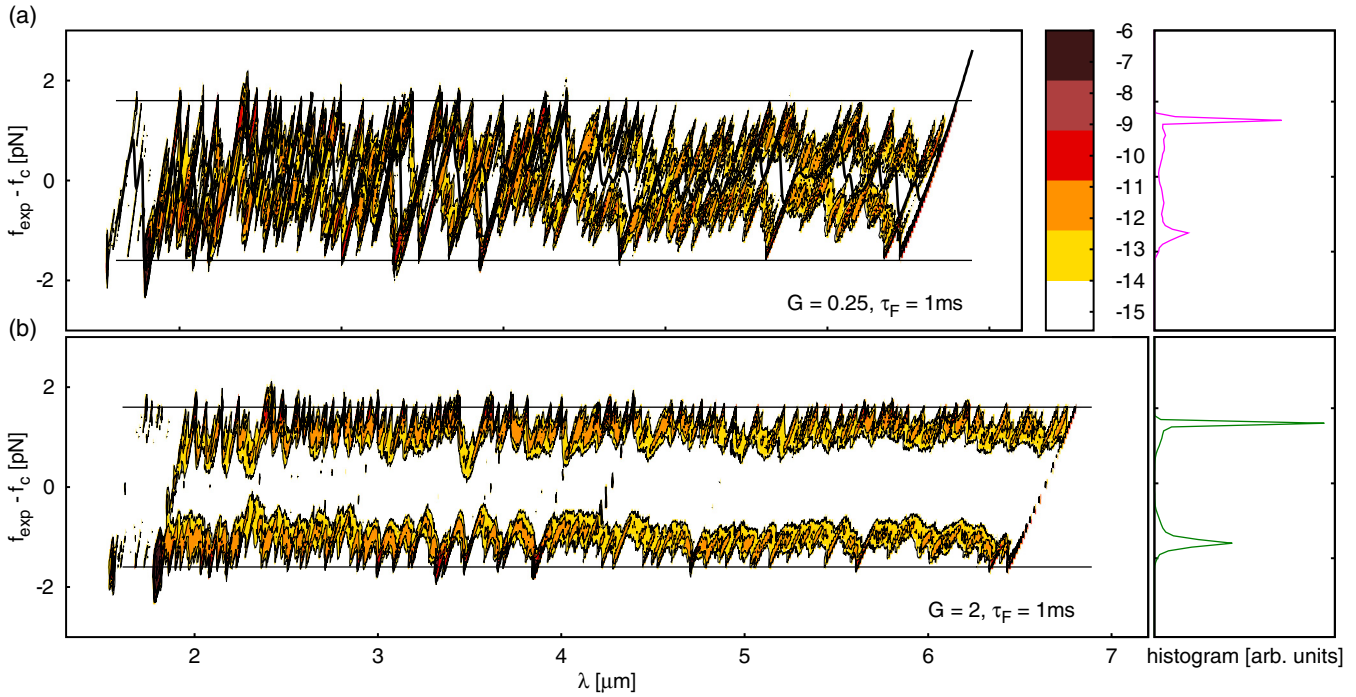

FIG. 7. Logarithm of the simulated probability density in the $(f_{\rm exp},\lambda)$ plane (left) and corresponding force histogram (right) for $f_c = 17.0$ pN, $\Delta f = 1.6$ pN, $\tau_e = 1.33$ s, $\tau_F = 1$ ms, and two values of G. In (a), we show the equilibrium FDC in black. The target values are represented by horizontal lines.

to generate. For this feedback gain, the feedback mechanism thus manages to keep the force variance sufficiently small to resolve both target forces.

The experimental results are again compared to simulation outcomes, showing qualitative agreement of theory and experiment (see Figs. 6 and 7). The experimental probability densities naturally offer a lower resolution due to additional noise sources not included in the simulation such as the damping motion of the mechanically coupled fiber wiggler and drift effects. Still, the region of the most populated forces is pushed away from equilibrium and towards the target force values for larger G in both the experiments and the simulations. In particular, the good agreement of the simulated probability density in the $(f_{\rm exp},\lambda)$ plane with the equilibrium FDC for small G supports the experimental observation that the system equilibrates if the feedback is weak [Fig. 7(a)].

V. CONCLUSION

We have considered the dynamics of a single DNA hairpin that is stochastically driven by a force feedback mechanism. With the force relaxation after a change of the target force and the probability density in the $(f_{\rm exp},\lambda)$ plane we have established two quantities that allow us to evaluate the feedback-controlled dynamics. For the force relaxation, an analytic expression has been derived for a simple toy model where the complex DNA unfolding landscape is replaced by a harmonic oscillator. This expression emphasizes that the time evolution of the mean force after a change of the target force depends critically on the value of the feedback gain G. In particular, the system becomes unstable if G is too large.

For the DNA hairpin, experiments and simulations show that the force relaxation after a change of the target force is more complex since more time scales contribute to the dynamics. We stress that this kind of force relaxation is not only found for the stochastic driving protocol investigated here but can be similarly observed for a constant-force feedback protocol where the relaxation of the mean force occurs after conformational transition events that quickly change the force. This is the case in constant-force hopping experiments where force feedback can modify the values of intrinsic constant-force rates [13,14,32].

The discussion of the probability density in the $(f_{\rm exp},\lambda)$ plane makes the need for the feedback to counteract the system equilibration most explicit. Comparing this probability density with the force-distance curve from an equilibrium unfolding process demonstrates that the system inevitably equilibrates if the feedback adjustments are weak. For larger feedback gains G, these adjustments are stronger, allowing the feedback to push the system further into the nonequilibrium regime.

The discussion of the DNA unfolding process under feedback control, which we have performed here in both theory and experiment, hence highlights that the dynamics of the DNA hairpin depends strongly on the parameter of the feedback mechanism. Thus, our study helps to establish the DNA unfolding process as a nontrivial paradigm, which can be used to address general topics raised in the field of feedback mechanisms for small complex systems. In future work, the DNA unfolding process could therefore be used to, e.g., paradigmatically discuss how quantities that have increasingly attracted interest in recent years, such as the mutual information connected with a measurement, depend on the parameters of the feedback mechanism.

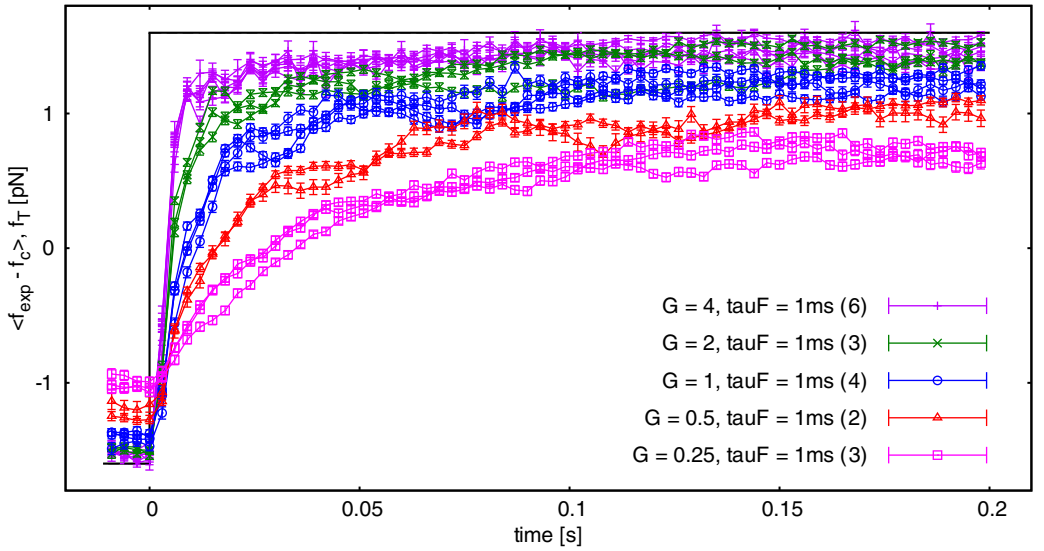

FIG. 8. Experimental force relaxation after a change of the target force from $f_T^- = f_c - \Delta f$ to $f_T^+ = f_c + \Delta f$ (black), for $f_c \simeq 18.1$ pN, $\Delta f = 1.6$ pN, $\tau_e = 1.33$ s, $\tau_F = 1$ ms, and various G. Each trajectory corresponds to a single molecule. For each value of G, the number in brackets is the number of single molecules measured.

ACKNOWLEDGMENTS

E.D. thanks Jan Reinke for his assistance in setting up the simulations of the long DNA hairpin under feedback control. F.R. is supported by an Institució Catalana de Recerca i Estudis Avançats (ICREA) Academia 2013 grant. The research leading to these results (J.C.-S., M.R.-C., F.R.) has received funding from the European Union Seventh Framework Programme (FP7/2007-2013) under Grants No. 308850 INFERNOS (Information, Fluctuations, and Energy Control in Small Systems) and No. FIS2013-47796-P from the Spanish Research Council.

E.D. and J.C.-S. contributed equally to this work.

APPENDIX: SINGLE-MOLECULE RESULTS

Figure 8 shows single-molecule results of the force relaxation after a change of the target force. These

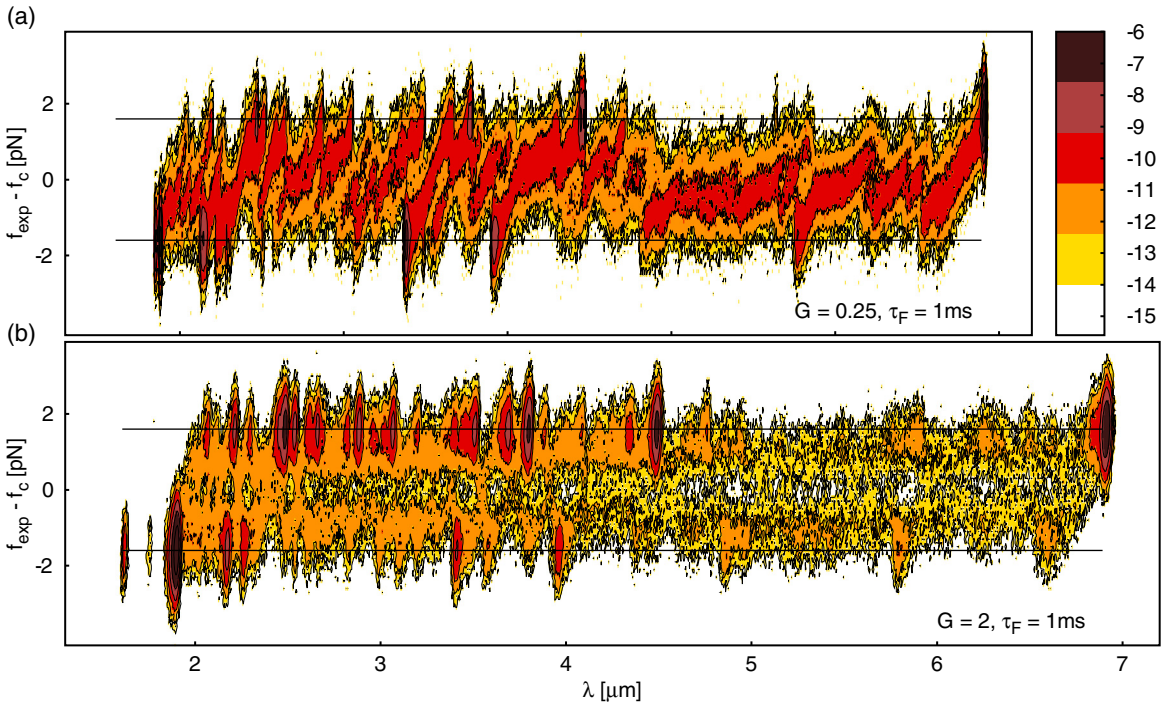

FIG. 9. Logarithm of the experimental single molecule probability density in the $(f_{\rm exp}, \lambda)$ plane for $f_c \simeq 18.1$ pN, $\Delta f = 1.6$ pN, $\tau_e = 1.33$ s, $\tau_F = 1$ ms, and two values of G. The target values are represented by horizontal lines.

results have been used to calculate the single-molecule averages presented in Fig. 5. The remarkable agreement of different experiments performed with the same parameters highlights the consistency of the experimental data.

Furthermore, in Fig. 9, we show one randomly selected single-molecule result for each feedback gain for which a single-molecule average is given in Fig. 6 to emphasize that experiments at the same parameters have been consistent for the probability density in the $(f_{\mathrm{exp}},\lambda)$ plane as well.

[1] S. B. Smith, Y. J. Cui, and C. Bustamante, Science **271**, 795 (1996).
[2] M. Rief, M. Gautel, F. Oesterhelt, J. M. Fernandez, and H. E. Gaub, Science **276**, 1109 (1997).
[3] C. Bustamante, J. Liphardt, and F. Ritort, Phys. Today **58**, 43 (2005).
[4] S. Ciliberto, S. Joubaud, and A. Petrosyan, J. Stat. Mech. (2010) P12003.
[5] V. Blickle and C. Bechinger, Nature Phys. **8**, 143 (2012).
[6] J. P. Pekola, Nature Phys. **11**, 118 (2015).
[7] J. R. Moffitt, Y. R. Chemla, S. B. Smith, and C. Bustamante, Biochemistry **77**, 205 (2008).
[8] K. C. Neuman and A. Nagy, Nature Methods **5**, 491 (2008).
[9] G. J. Wuite, S. B. Smith, M. Young, D. Keller, and C. Bustamante, Nature (London) **404**, 103 (2000).
[10] S. B. Smith, Y. Cui, and C. Bustamante, Methods Enzymol. **361**, 134 (2002).
[11] W. J. Greenleaf, M. T. Woodside, E. A. Abbondanzieri, and S. M. Block, Phys. Rev. Lett. **95**, 208102 (2005).
[12] A. R. Carter, Y. Seol, and T. T. Perkins, Biophys. J. **96**, 2926 (2009).
[13] J. D. Wen, M. Manosas, P. T. X. Li, S. B. Smith, C. Bustamante, F. Ritort, and I. Tinoco, Biophys. J. **92**, 2996 (2007).
[14] M. Manosas, J. D. Wen, P. T. X. Li, S. B. Smith, C. Bustamante, I. Tinoco, and F. Ritort, Biophys. J. **92**, 3010 (2007).
[15] B. Ibarra, Y. R. Chemla, S. Plyasunov, S. B. Smith, J. M. Lazaro, M. Salas, and C. Bustamante, The EMBO Journal **28**, 2794 (2009).
[16] J. Camunas-Soler, M. Manosas, S. Frutos, J. Tulla-Puche, F. Albericio, and F. Ritort, Nucleic Acids Research **43**, 2767 (2015).
[17] J. V. Koski, V. F. Maisi, J. P. Pekola, and D. V. Averin, Proc. Nat. Acad. Sci. **111**, 13786 (2014).
[18] S. Toyabe, T. Sagawa, M. Ueda, E. Muneyuki, and M. Sano, Nature Phys. **6**, 988 (2010).
[19] R. Landauer, IBM J. Res. Develop. **5**, 183 (1961).
[20] A. Berut, A. Arakelyan, A. Petrosyan, S. Ciliberto, R. Dillenschneider, and E. Lutz, Nature (London) **483**, 187 (2012).
[21] Y. Jun, M. Gavrilov, and J. Bechhoefer, Phys. Rev. Lett. **113**, 190601 (2014).
[22] E. Dieterich, J. Camunas-Soler, M. Ribezzi-Crivellari, U. Seifert, and F. Ritort, Nature Phys. **11**, 971 (2015).
[23] J. Bechhoefer, Rev. Mod. Phys. **77**, 783 (2005).
[24] T. Sagawa and M. Ueda, Phys. Rev. Lett. **104**, 090602 (2010).
[25] D. Abreu and U. Seifert, Europhys. Lett. **94**, 10001 (2011).
[26] P. Strasberg, G. Schaller, T. Brandes, and M. Esposito, Phys. Rev. Lett. **110**, 040601 (2013).
[27] A. C. Barato and U. Seifert, Phys. Rev. Lett. **112**, 090601 (2014).
[28] J. M. R. Parrondo, J. M. Horowitz, and T. Sagawa, Nature Phys. **11**, 131 (2015).
[29] M. L. Rosinberg, T. Munakata, and G. Tarjus, Phys. Rev. E **91**, 042114 (2015).
[30] J. M. Huguet, C. V. Bizarro, N. Forns, S. B. Smith, C. Bustamante, and F. Ritort, Proc. Natl. Acad. Sci. **107**, 15431 (2010).
[31] J. M. Huguet, N. Forns, and F. Ritort, Phys. Rev. Lett. **103**, 248106 (2009).
[32] P. J. Elms, J. D. Chodera, C. J. Bustamante, and S. Marqusee, Biophys. J. **103**, 1490 (2012).